Applied Nanoscience (2023) 13:3819–3826
https://doi.org/10.1007/s13204-022-02560-0

ORIGINAL ARTICLE

Pyramid-shaped MMn_2O_4/rGO (M = Ni, Co) nanocomposites and their application in ammonia sensors

G. Marimuthu[1] · G. Bharathi[2] · G. Palanisamy[3] · Munirah D. Albaqami[4] · Abdulnasser Mahmoud Karami[4] · G. Mani[5] · T. Pazhanivel[1]

Received: 28 January 2022 / Accepted: 10 July 2022 / Published online: 27 July 2022

Abstract

Herein, the MMn_2O_4 and MMn_2O_4/rGO (M = Ni, Co) samples were synthesized using co-precipitation and wet impregnation methods. XRD analysis showed the high purity and good crystallinity of the synthesized powders. FESEM analysis revealed the formation of pyramid-like structures and a good intimate mixture with rGO in the nanocomposite samples. Gas sensors were fabricated with pure and nanocomposite structures for the sensing of ammonia gas. The $CoMn_2O_4$/rGO nanocomposite sample achieved a higher sensitivity ($S = 3.5$) with shorter response/recovery (140 s/83 s) behavior in room temperature at 100 ppm of NH_3. The stability and selectivity of the $CoMn_2O_4$/rGO nanocomposite gas sensor were examined. The preferable sensing mechanism of $CoMn_2O_4$/rGO nanocomposite towards the detection of NH_3 was discussed.

Keywords rGO · $NiMn_2O_4$/rGO nanocomposite · $CoMn_2O_4$/rGO nanocomposite · Ammonia sensor · Wet impregnation method

Introduction

Today, urbanization and industrial growth continually produce emissions of different poisoning and harmful gases. It is highly important to maintain a safe living environment, in such a way that the industrial revolution should not affect our day-to-day life. To maintain safe living standards, hazardous emissions need to be monitored continuously, and sensors are the heart of these precautions. Gas sensors are inevitable since they can monitor hazardous emissions in real-time, and help us to take immediate actions if required. Gas sensors that are made up of semiconductor metal oxide micro/nanomaterials have gained more interest due to their salient features such as high sensitivity, selectivity, low cost, and simplicity in manufacturing. Transition metal oxides as electrode materials are nevertheless limited by their fast sensing response with high operation temperatures, but due to low conductivity and the aggregation problem that arises from the preparation methods. Several nanostructured transition metal oxides, such as $NiFe_2O_4$ (Song et al. 2018; Paquin et al. 2015), MCo_2O_4 (M = Mn, and Zn) (Zhou et al. 2019), $NiCo_2O_4$ (Dang et al. 2020), and so on, have been investigated.

Graphene has gained tremendous attention due to its preeminent electrical features. The graphene samples prepared by vapor deposition carry most of the features and are compatible to construct a variety of nanoscale devices. However, the problem arises when it comes to mass production. Alternatively, the exfoliation-based chemical routes provide an avenue for high volume synthesis, but with few compromises in the graphitic carbon skeleton. In other words, the chemically prepared graphene samples may have several defects in the graphitic carbon structure, and there could be

✉ T. Pazhanivel
pazhanit@gmail.com

1 Smart Materials Interface Laboratory, Department of Physics, Periyar University, Salem, Tamil Nadu 636011, India

2 Key Laboratory of Optoelectronic Devices and Systems of Guangdong Province, College of Optoelectronic Engineering, Shenzhen University, Shenzhen 518060, Guangdong Province, People's Republic of China

3 SSN Research Centre, Sri Sivasubramaniya Nadar College of Engineering, Kalavakkam, Chennai 603 110, Tamil Nadu, India

4 Department of Chemistry, College of Science, King Saud University, Riyadh 11451, Saudi Arabia

5 Korea University of Technology and Education, Cheonan-si 31253, Chungcheongnam-do, Republic of Korea

several layers if exfoliation is not done properly. The defects in the chemically exfoliated graphene sample, which is technically known as graphene oxide, can be reduced/restored by the post-synthesis reduction processes. Such reduced samples are known as reduced graphene oxide (rGO) and are closely comparable to the vapor phase-grown graphene samples. Another important point to note here is, the chemically prepared graphene samples always have several functional groups at the edges, which have both positive and negative effects on case-to-case basis. In the case of composite preparation, these functional groups can act as anchoring sites for the compositing counterparts.

According to previous studies, Qiuxia Fend et al. (2015) synthesized the rGO-loaded Co_3O_4 using the electrospinning technique, at room temperature. It showed a tenfold stronger response to NH_3 gas than the pristine gas sensor. Veena Mounasamy et al. (Jeevitha et al. 2019) prepared rGO/WO_3 nanocomposites by an ultrasonication method. Their ammonia gas sensing property at room temperature was studied. The results showed that the rGO/WO_3 nanocomposites exhibited a response time of 17 s and recovery time of 21 s for 14 ppm of ammonia. Similarly, Priyabrat Dash et al. (Achary et al. 2018) used the combination of $CuFe_2O_4$ with rGO, which resulted in the improvement of ammonia (NH_3) sensing response by 25% for 200 ppm and 2% for 5 ppm.

Here, pure MMn_2O_4 and MMn_2O_4/rGO (M = Ni, Co) pyramid-shaped nanocomposites were successfully prepared through the co-precipitation and wet impregnation methods. The gas-sensing performance of MMn_2O_4/rGO (M = Ni, Co) composites against ammonia gas was investigated in detail. The $NiMn_2O_4$ and $CoMn_2O_4$ pyramids can provide a large specific surface area for gas sensing performances. The composite formation with rGO sheets not only offers electron conductive channels but also prevents the active materials from aggregating.

Experiment section

Manganese nitrate tetrahydrate ($Mn(NO_3)_2{\cdot}4H_2O$), Nickel nitrate hexahydrate ($Ni(NO_3){\cdot}6H_2O$), Cobalt nitrate hexahydrate ($Co(NO_3)_2{\cdot}4H_2O$) and sodium hydroxide (NaOH) were purchased merck and used without any further purification process. Double-distilled water (DDW) was used as the solvent and the enhanced hummers' process was used to synthesize graphite oxide.

Preparation of rGO

In brief, GO (graphene oxide) was prepared from purified natural graphite through the modified Hummers method. In this method, 5 g of graphite, 2.5 g of $NaNO_3$, and 115 ml of concentrated H_2SO_4 were mixed for 4 h in an ice bath with steady stirring. Following that, 15 g of $KMnO_4$ was gently added to the above-mentioned mixture for around 20 min. The ice bath was removed after mixing, and the suspension was agitated for another 2 h. The suspension was then heated in a water bath at 98 °C for 15 min after adding 230 ml of distilled water dropwise. It was diluted again with 400 ml warm water and then 20 ml H_2O_2 (30%) was added dropwise. The mixture was then centrifuged at 4000 rpm and rinsed with HCl aqueous solution (10%) followed by distilled water. Finally, it was dialysis filtered for 3 h until the pH was neutral, then dried in air at room temperature (Du et al. 2016; Amir Faiz et al. 2020). Finally, we crushed the yield and obtained the GO powder (~ 3 g).

In a typical procedure, for the preparation of rGO, 1 g of GO was dispersed in 50 ml of water and sonicated for 1 h and then 20 ml of ammonia solution was added dropwise into the solution, forming a smooth brown dispersion of graphene oxide. After that, the aqueous solution was moved to a Teflon-lined autoclave and heated at 180 °C for 6 h. The autoclave was then cooled to room temperature and the resulting product was separated by centrifugation, washed with plenty of water, and dried at 60 °C for 12 h (Nasresfahani et al. 2017).

Preparation of $NiMn_2O_4$, $CoMn_2O_4$, $NiMn_2O_4$/rGO and $CoMn_2O_4$/rGO

In this study, $NiMn_2O_4$ was prepared using the co-precipitation method. First, 10.92 g of $Mn(NO_3)_2{\cdot}4H_2O$, was dissolved in 80 ml of distilled water under stirring for 30 min. Secondly, 5.68 g of $Ni(NO_3){\cdot}6H_2O$, was added to the above solution to form a homogeneous mixture, and then the temperature was increased to 90 °C. To achieve the pH value of 12, sodium hydroxide (NaOH, 2 M) was added drop-wise to the obtained aqueous solution. After 90 min, the precipitates were centrifuged and washed with double-distilled water, and then dried at 100 °C for 24 h. The dried product was ground into a fine powder and annealed at 900 °C for 3 h. The same process was repeated to prepare pure $CoMn_2O_4$ (5 g), but using $Co(NO_3){\cdot}6H_2O$ (Marimuthu et al. 2020).

$NiMn_2O_4$/rGO and $CoMn_2O_4$/rGO composite were prepared by the wet impregnation method (Palanisamy et al. 2018). 0.5 g of $NiMn_2O_4$ and 0.05 g of rGO samples were added separately into 15 ml of ethanol. The resulting solution was continuously stirred and subsequently heated at 60 °C to evaporate the solvent. Then, the obtained $NiMn_2O_4$/rGO composite was dried for 6 h, collected and stored for further processes. The same process was repeated to prepare $CoMn_2O_4$/rGO (Paquin et al. 2015).

Gas-sensing device fabrication and measurements

The gas sensing material was prepared by dispersing the annealed powder samples in ultrapure water by ultrasonic agitation for 30 min. The dispersed suspension was then spread over a Fluorine doped tin oxide (FTO) coated glass substrate and dried at 80 °C for 3 h. The gas sensing properties were measured using a pico ammeter (standard deviation error ± 1) connected to the sensor, which is kept inside a chamber (Type and Chandra 2017). In a sealed testing box, the mounted sensors were positioned, where various concentrations of target gas can be delivered. The response to the reducing gas by MMn_2O_4/rGO (M = Ni, Co) gas sensors was equal to the value of $S = I_g/I_a$, where I_g was the sensor current for different target gas concentrations and I_a was the sensor current for open-air atmosphere (Rathore et al. 2013; Gusain et al. 2017).

Results and discussion

XRD analysis

Figures 1 and 2 present the XRD patterns of rGO, $NiMn_2O_4$, $NiMn_2O_4$/rGO, $CoMn_2O_4$, and $CoMn_2O_4$/rGO samples. In the rGO sample (Fig. 1), the peaks located at 25.6°, 44.55° and 55.2° were contributed by the (002), (110), and (004) planes of rGO, respectively, which is according to the JCPDS card No. 75-2078 (Munde et al. 2020). The observed peak broadness at 25.6° could be interpreted as the presence of nanofragments of rGO and oxygen-containing functional groups such as carbonyl, hydroxyl, and epoxy on the surface/edges of rGO, which play as anchoring sites for

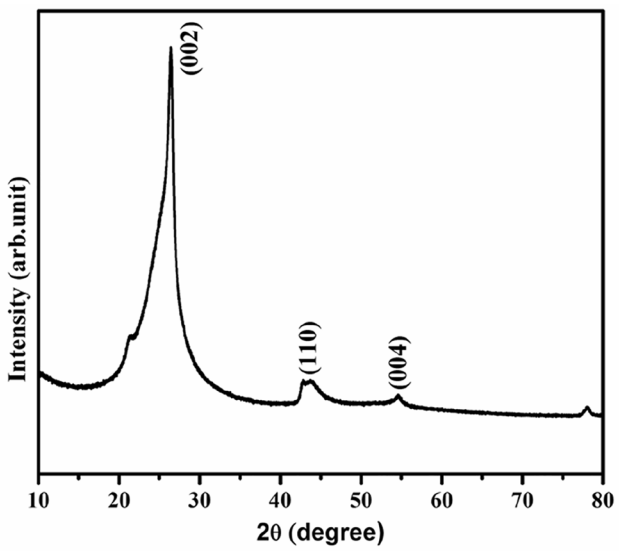

Fig. 1 XRD pattern of rGO

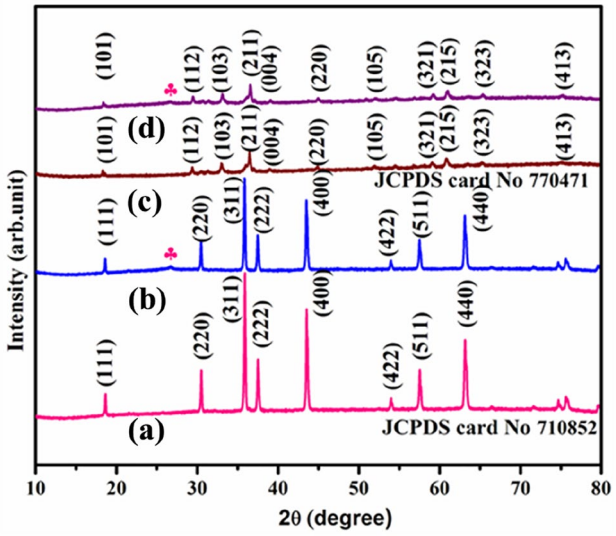

Fig. 2 XRD patterns of **a** $NiMn_2O_4$, **b** $NiMn_2O_4$/rGO, **c** $CoMn_2O_4$, and **d** $CoMn_2O_4$/rGO nanocomposite

metal oxides. As shown in Fig. 2a, b the diffraction peaks of $NiMn_2O_4$ at 18.1°, 30.8°, 35.4°, 37.4°, 53.03°, 43.03°, 56.9°, and 62.4° correspond to the (111), (220), (311), (222), (400), (422), (511), and (440) crystal planes of $NiMn_2O_4$, respectively, which is in accordance with the JCPDS card No. 710852 (Gawli et al. 2014).

The characteristic peaks of $NiMn_2O_4$ were also observed in the case of the $NiMn_2O_4$/rGO composite sample (Fig. 2b), along with the diffraction peak of rGO, which confirms the formation of the $NiMn_2O_4$/rGO composite (Gawli et al. 2014; Li and Yang 2020). In Fig. 2c, the diffraction peaks of $CoMn_2O_4$ at 18.1°, 29.3°, 30.8°, 33.3°, 36.7°, 36.8°, 44.2°, 51.07°, 52.7°, 53.9°, and 60.8° corresponding to the (101), (112), (103), (211), (004), (220), (105), (321), (215), (323), and (413) crystal planes of cubic $CoMn_2O_4$, are consistent with the JCPDS card No. 770471. The observation of diffraction peaks corresponding to both $CoMn_2O_4$ and rGO in the case of the $CoMn_2O_4$/rGO sample (Fig. 2d), confirms the successful formation of the nanocomposite (Su et al. 2020).

FTIR analysis

The FTIR spectrum of rGO, $NiMn_2O_4$, $NiMn_2O_4$/rGO, $CoMn_2O_4$, and $CoMn_2O_4$/rGO samples are shown in Fig. 3. The FTIR spectrum of rGO (Fig. 3a) showed a peak at 1560 cm^{-1} originated from C=C structure of graphene sheets and the peak at 1190 cm^{-1} was attributed to C–OH stretching. The $NiMn_2O_4$ and $NiMn_2O_4$/rGO samples (Fig. 3b, c) displayed two intensive bands at around 531 cm^{-1} and 621 cm^{-1}, which were caused by the Ni^{2+} and Mn^{3+}/Mn^{4+} (Gawli et al. 2014). The observed reduction in the intensity of C=O stretching vibrational band at

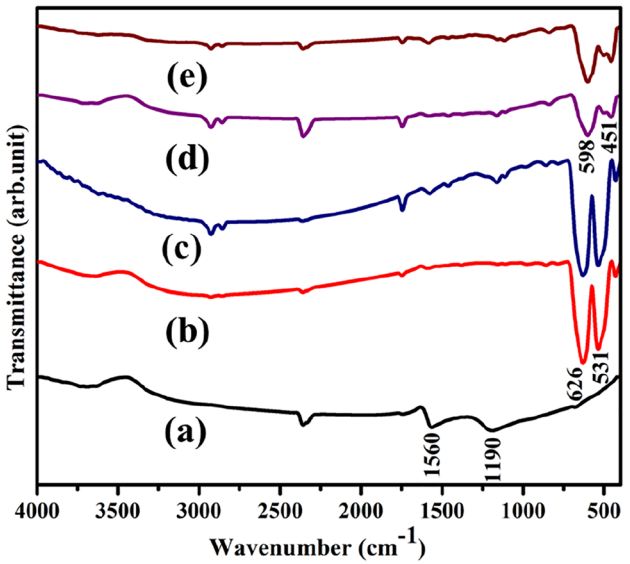

Fig. 3 FTIR transmittance spectra of **a** rGO, **b** $NiMn_2O_4$, **c** $NiMn_2O_4$/rGO, **d** $CoMn_2O_4$ and **e** $CoMn_2O_4$/rGO nanocomposite

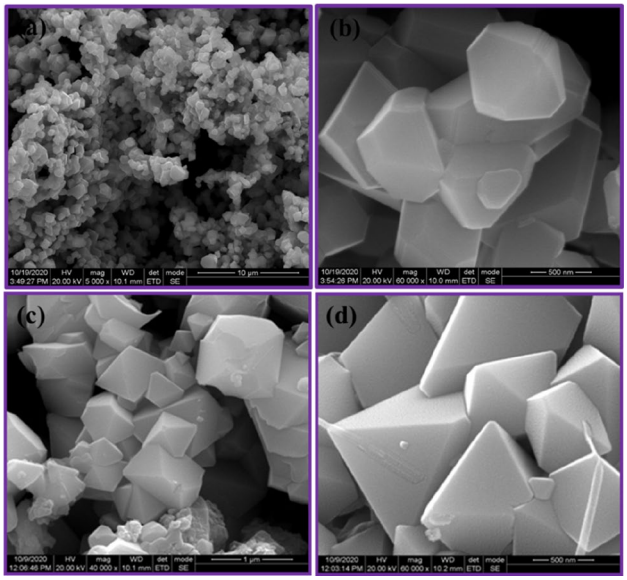

Fig. 4 FESEM images of **a**, **b** $NiMn_2O_4$, and **c**, **d** $CoMn_2O_4$

1737 cm^{-1} in the $NiMn_2O_4$/rGO sample (Fig. 3c), confirms the nanocomposite formation (Manuscript 2015). Similarly, the FTIR spectrum of $CoMn_2O_4$ and $CoMn_2O_4$/rGO samples presented in Fig. 3d, e contained two peaks in the lower wavenumber region (451 cm^{-1} and 598 cm^{-1} corresponding to Co^{2+} and Mn^{3+}/Mn^{4+}-O^{2-}), confirming the presence of metal–oxygen stretching vibrations. In addition, few peaks were observed in common for all the samples. The peak observed at 2922 cm^{-1} is attributed to the surface-adsorbed CO_2 molecule from the atmosphere (Sahoo et al. 2016; Hu et al. 2019). The broad peak at around 3421 cm^{-1} corresponds to OH stretching vibrations of H_2O molecules (Saranya and Selladurai 2018).

Morphological characterization

FESEM was employed to investigate the morphologies of the pure and rGO composited metal oxide samples. The FESEM images of pure $NiMn_2O_4$ and $CoMn_2O_4$ presented in Fig. 4a–d, show the formation of regularly shaped particles. The $NiMn_2O_4$ samples (Fig. 4a, b) exhibit a morphology like a 3D hexagon with irregular thickness. The $CoMn_2O_4$ sample exhibit a well-grown pyramid-like structure (given in Fig. 4c, d) (Samodi et al. 2013). As reported elsewhere, the wet impregnation method is a simpler and one of the best methods for preparing graphene-based composites (Sun et al. 2019).

In the present case, using the wet impregnation process, the $NiMn_2O_4$ and $CoMn_2O_4$ nanoparticles were anchored over the rGO layers, which was expected to help in improving the gas sensing performances of the prepared samples. The presence of exfoliated rGO sheets covered with MMn_2O_4 (M = Ni, Co) is shown in Fig. 5. Both the $NiMn_2O_4$/rGO (Fig. 5a, b) and $CoMn_2O_4$ (Fig. 5c, d) samples show the incorporation of MMn_2O_4 with rGO.

Gas sensing performance

In general, sensing materials with suitable nanostructures, such as nanoparticles, nanowires, nanoflower, etc., produce better gas sensors (Bhati et al. 2020). The design of special

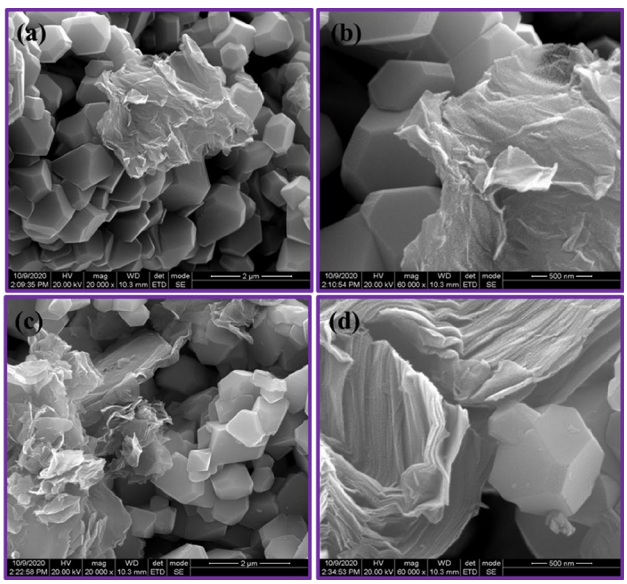

Fig. 5 FESEM images of **a**, **b** $NiMn_2O_4$/rGO, and **c**, **d** $CoMn_2O_4$/rGO nanocomposite

forms/structures (morphology) in the sensing surface has been considered by researchers as a possible method for achieving good results (Li et al. 2019). For example, Yi Zeng et al., reported a sensing response of 0.6 using $CoFe_2O_4$ double-shelled hollow spheres towards ammonia at room temperature (Wang et al. 2020).

The gas sensing performance (current versus time) of the prepared samples was investigated (at 30 °C) by admitting 100 ppm of NH_3 into the gas sensing chamber equally for each sample, and the sensing response was determined by measuring the current value. As shown in Fig. 6a, the sensitivity of the samples was calculated to be 1.03 and 1.5, for the pure $NiMn_2O_4$ and $CoMn_2O_4$ samples, respectively. The calculated sensitivity values increased for the case of composite samples to 1.55 and 3.5, for $NiMn_2O_4$/rGO and $CoMn_2O_4$/rGO, respectively. The sensitivity value for the $CoMn_2O_4$/rGO sample was surprisingly higher when compared to the other samples. This can be attributed to the presence of a greater number of active sites for oxygen adsorption along with the charge transfer channel (rGO), in the corresponding sample. The sensing performances of the $CoMn_2O_4$/rGO sample were further examined by admitting different concentrations of NH_3 (10 to 100 ppm), and the results are shown in Fig. 6b.

The selectivity of the $CoMn_2O_4$/rGO gas sensor was investigated by exposing 100 ppm of various gases such as ammonia (NH_3), ethanol (CH_3CH_2OH), and acetone (CH_3COCH_3). The selectivity characteristic results for the $CoMn_2O_4$/rGO sample are displayed in Fig. 6c. It is observed that the sensor was selective towards ammonia gas at room temperature, with the highest sensitivity value of 3.5. The $CoMn_2O_4$/rGO sensor's long-term stability was also examined by repeating the sensing measurement with 10 cycles of exposure and the results are presented in Fig. 6d. The sensor was found to have only a slight reduction in the sensing response. The obtained results have therefore revealed that the $CoMn_2O_4$/rGO gas sensor has long-term stability for repeated cycling detections. Figure 7 shows the response and recovery times of the $CoMn_2O_4$/rGO gas sensor against various concentrations of NH_3 (10–100 ppm). The response time increased from 60 s to around 140 s with the increase of gas concentration. A reason for more number of NH_3 gas molecules that get adsorbed on the sensor surface reacting with the $CoMn_2O_4$/rGO. The recovery time was initially higher, which increased first from 120 to around 150 s. However, beyond 50 ppm the recovery time decreased and reached 83 s, for the ammonia concentration of 100 ppm. Table 1 shows a comparison of the gas sensing response of $CoMn_2O_4$/rGO nanocomposite recognized sensor with the other previous reported NH_3 sensors.

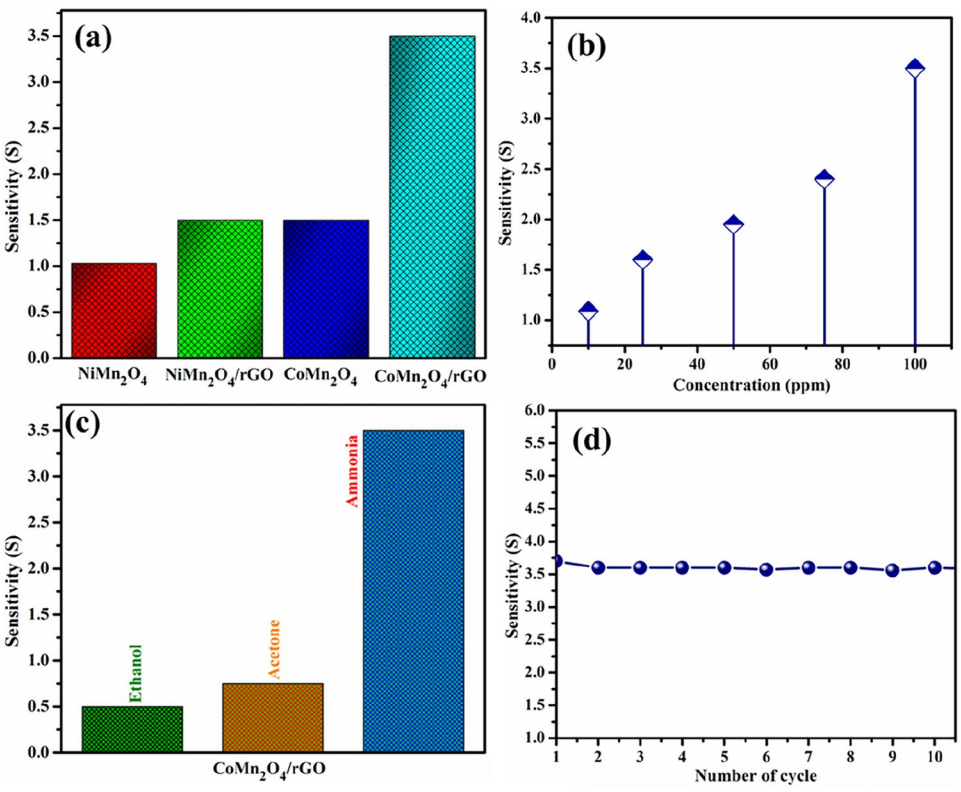

Fig. 6 **a** Comparison of sensitivity of MMn_2O_4 (M = Ni, Co), and MMn_2O_4/rGO (M = Ni, Co)/rGO, to 100 ppm NH_3 gas. **b** gas sensing response of the $CoMn_2O_4$/rGO to different concentrations of NH_3. **c** Comparison of gas sensing response of the $CoMn_2O_4$/rGO towards different gases. **d** Stability of the $CoMn_2O_4$/rGO sensor to NH_3 up to 10 cycles

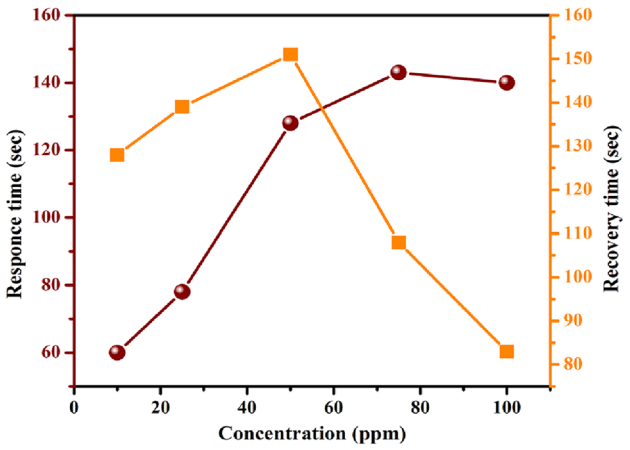

Fig. 7 Response and recovery time curve of $CoMn_2O_4$/rGO sample

Sensing mechanism

It is well known that the principle mechanism for gas detection is based on the adsorption–desorption of molecules on the sensor surface (Sovizi 2020). Several reports have been published to demonstrate the functionality of these types of sensors. In the present case, the surface of $CoMn_2O_4$/rGO consists of a large number of hetero-nanograins, on which the O_2 molecules in air get adsorbed to effect the change in current. In detail, the oxygen molecules adsorbed on the surface of $CoMn_2O_4$/rGO nanocomposite, arrest free electrons from the conduction band to form O^{2-} oxygen ions (Qin et al. 2014). This creates free-electron deficiency and consequently the current flow is restricted. The current produced by $CoMn_2O_4$/rGO nanocomposite sensor, at this stage is primarily influenced by the formation of oxygen ions and is known as the initial current or base current of the sensor (I_a). When the analyte gas, i.e., ammonia gas is admitted, it reacts with the surface adsorbed oxygen ions, which results in the release of free electrons to the conduction band of the $CoMn_2O_4$/rGO sensor. This release of free electrons increases the current flow, which is now recorded as I_g. The recorded values of I_g and I_a can be used to calculate the sensitivity.

The oxygen ion formation on the sensor surface can be regulated by controlling the operating temperature, for example, only the O^{2-} (< 100 °C) and O^- (100–300 °C) ions can be chemically formed at relatively low temperatures (Kumar and Mariappan 2019).

The following equations demonstrate the general possible reaction in $CoMn_2O_4$/rGO during ammonia gas sensing.

$$O_2(\text{gas}) \rightarrow O_2(\text{adsorb}) \quad (1)$$

$$O_2(\text{adsorb}) + e^- \rightarrow O^2(\text{adsorb}) \quad (2)$$

$$4NH_3 + 5O^{2-}(\text{adsorb}) \rightarrow 4NO + 6H_2O + 5e^- \quad (3)$$

The ammonia gas gets oxidized by reacting with oxygen ions, as mentioned in Eq. (3). The selective oxidation-based ammonia sensing has been reported by several researchers. For example, Lihua Hub et al. (Dong et al. 2017) reported the room temperature ammonia sensing by hydrothermally synthesized coral-shaped Dy_2O_3, in which the sensor acted as a catalyst and oxidized the ammonia gas into NO and H_2O. Several catalysts, particularly, transition metal oxides such as Ag/Al_2O_3, MnO_x/CeO_2, La-hexaaluminates (La-M, where M = Fe, Cu, Co, and Mn) catalysts (Zhang and He 2009; Yu et al. 2015; Jiang et al. 2020), etc., have been investigated by the researchers, which gives hydrazinium-type intermediate during the oxidation of ammonia. In this study, the reducing gas (NH_3) is passed over the sensor ($CoMn_2O_4$/rGO), where it interacts with the adsorbed oxygen anions, causing the removal of oxygen from the sensor surface and as a result, the electrons got released back into the nanograins (Jain et al. 2018).

Conclusion

Highly sensitive ammonia (NH_3) gas sensor based on the $CoMn_2O_4$ pyramid decorated rGO nanosheet sample was fabricated. The micro/nano networks of $CoMn_2O_4$ pyramids were anchored homogeneously on the surface of reduced graphene oxide (rGO). The NH_3 sensing performances of the synthesized samples were examined with different gas concentrations. The $CoMn_2O_4$/rGO nanocomposite sample displayed excellent performance (3.5 for 100 ppm at room temperature) compared to the $NiMn_2O_4$ (1.03), $CoMn_2O_4$

Table 1 Comparison of gas sensing properties of $CoMn_2O_4$/rGO-based sensors with other NH_3 sensors

Sensing materials	T (°C)	Concentration (ppm)	Response (S)	Refs
TeO_2	170	500	58%	Siciliano et al. (2009)
In_2O_3:CuO	RT	0.3–100	1.6	Zhou et al. (2018)
$NiCo_2O_4$/r-GO	RT	100	1.068	Marimuthu et al. (2020)
GO-$CuFe_2O_4$	RT	5	2.35	Achary et al. (2018)
This work	RT	100	3.5	–

(1.5), and $NiMn_2O_4$/rGO (1.55) samples. The obtained results demonstrate that the pyramid-like $CoMn_2O_4$ nanostructure with rGO can be promising for the fabrication of high-performance gas sensor device.

Acknowledgements This work was funded by the Researchers Supporting Project Number (RSP-2021/267) King Saud University, Riyadh, Saudi Arabia.

Declarations

Conflicts of interest The authors declare that there are no conflicts of interest.

References

Achary LSK, Kumar A, Barik B et al (2018) Reduced graphene oxide-CuFe2O4 nanocomposite: a highly sensitive room temperature NH3 gas sensor. Sens Actuators B Chem 272:100–109. https://doi.org/10.1016/j.snb.2018.05.093

Amir Faiz MS, Che Azurahanim CA, Yazid Y et al (2020) Preparation and characterization of graphene oxide from tea waste and it's photocatalytic application of TiO2/graphene nanocomposite. Mater Res Express. https://doi.org/10.1088/2053-1591/ab689d

Bhati VS, Hojamberdiev M, Kumar M (2020) Enhanced sensing performance of ZnO nanostructures-based gas sensors: a review. Energy Rep 6:46–62. https://doi.org/10.1016/j.egyr.2019.08.070

Dang F, Wang Y, Gao J et al (2020) Hierarchical flower-like NiCo2O4 applied in n-butanol detection at low temperature. Sens Actuators, B Chem 320:128577. https://doi.org/10.1016/j.snb.2020.128577

Dong X, Cheng X, Zhang X et al (2017) A novel coral-shaped Dy2O3 gas sensor for high sensitivity NH3 detection at room temperature. Sens Actuators B Chem. https://doi.org/10.1016/j.snb.2017.08.117

Du F, Zuo X, Yang Q et al (2016) The stabilization of NiCo2O4 nanobelts used for catalyzing triiodides in dye-sensitized solar cells by the presence of RGO sheets. Sol Energy Mater Sol Cells 149:9–14. https://doi.org/10.1016/j.solmat.2015.11.025

Feng Q, Li X, Wang J, Gaskov AM (2015) Ac ce pt e t. Sens Actuators B Chem. https://doi.org/10.1016/j.snb.2015.09.021

Gawli Y, Badadhe S, Basu A et al (2014) Evaluation of n-type ternary metal oxide NiMn2O4 nanomaterial for humidity sensing. Sens Actuators, B Chem 191:837–843. https://doi.org/10.1016/j.snb.2013.10.071

Gusain A, Joshi NJ, Varde PV, Aswal DK (2017) Flexible NO gas sensor based on conducting polymer poly[N-9′-heptadecanyl-2,7-carbazole-alt-5,5-(4′,7′-di-2-thienyl-2′,1′,3′-benzothiadiazole)] (PCDTBT). Sens Actuators, B Chem 239:734–745. https://doi.org/10.1016/j.snb.2016.07.176

Hu Z, Zhou X, Lu Y et al (2019) CoMn2O4 doped reduced graphene oxide as an effective cathodic electrocatalyst for ORR in microbial fuel cells. Electrochim Acta 296:214–223. https://doi.org/10.1016/j.electacta.2018.11.004

Jain S, Patrike A, Badadhe SS et al (2018) Room-temperature ammonia gas sensing using mixed-valent $CuCo_2O_4$ nanoplatelets: performance enhancement through stoichiometry control. ACS Omega 3:1977–1982. https://doi.org/10.1021/acsomega.7b01958

Jeevitha G, Abhinayaa R, Mangalaraj D et al (2019) Porous reduced graphene oxide (rGO)/WO 3 nanocomposites for the enhanced detection of NH 3 at room temperature. Nanoscale Adv 1:1799–1811. https://doi.org/10.1039/C9NA00048H

Jiang G, Zhang F, Wei Z et al (2020) Selective catalytic oxidation of ammonia over LaMAl11O19-: δ (M = Fe, Cu Co, and Mn) hexaaluminates catalysts at high temperatures in the Claus process. Catal Sci Technol 10:1477–1491. https://doi.org/10.1039/c9cy02512j

Kumar V, Mariappan CR (2019) Characterization of mesoporous Zn doped NiCo2O4 rods produced by hydrothermal method for NOx gas sensing application. J Alloys Compd 773:158–167. https://doi.org/10.1016/j.jallcom.2018.09.264

Li M, Yang S (2020) Hybrids of nickel manganate nanosheets and nanoflowers on reduced graphene oxide for supercapacitors. Mater Lett 277:128270. https://doi.org/10.1016/j.matlet.2020.128270

Li Z, Li H, Wu Z et al (2019) Advances in designs and mechanisms of semiconducting metal oxide nanostructures for high-precision gas sensors operated at room temperature. Mater Horizons 6:470–506. https://doi.org/10.1039/c8mh01365a

Manuscript A (2015) Mater Chem A. https://doi.org/10.1039/C4TA05865H

Marimuthu G, Palanisamy G, Pazhanivel T et al (2020) NiCo2O4 functionalized with rGO catalyst as an active layer for ammonia sensing. Ionics (Kiel) 26:5233–5240. https://doi.org/10.1007/s11581-020-03598-2

Munde AV, Mulik BB, Dighole RP, Sathe BR (2020) Cobalt oxide nanoparticle-decorated reduced graphene oxide (Co3O4-rGO): active and sustainable nanoelectrodes for water oxidation reaction. New J Chem 44:15776–15784. https://doi.org/10.1039/d0nj02598d

Nasresfahani S, Sheikhi MH, Tohidi M, Zarifkar A (2017) Methane gas sensing properties of Pd-doped SnO2/reduced graphene oxide synthesized by a facile hydrothermal route. Mater Res Bull 89:161–169. https://doi.org/10.1016/j.materresbull.2017.01.032

Palanisamy G, Bhuvaneswari K, Bharathi G et al (2018) Enhanced photocatalytic properties of ZnS-WO3 nanosheet hybrid under visible light irradiation. ChemistrySelect 3:9422–9430. https://doi.org/10.1002/slct.201801688

Paquin F, Rivnay J, Salleo A et al (2015) Multi-phase semicrystalline microstructures drive exciton dissociation in neat plastic semiconductors. J Mater Chem C 3:10715–10722. https://doi.org/10.1039/b000000x

Qin N, Xiang Q, Zhao H et al (2014) Evolution of ZnO microstructures from hexagonal disk to prismoid, prism and pyramid and their crystal facet-dependent gas sensing properties. CrystEngComm16:7062–7073. https://doi.org/10.1039/c4ce00637b

Rathore D, Kurchania R, Pandey RK (2013) Sensors and actuators a: physical fabrication of Ni 1–x Zn x Fe_2O_4 (x = 0, 0. 5 and 1) nanoparticles gas sensor for some reducing gases. Sens Actuators A Phys 199:236–240. https://doi.org/10.1016/j.sna.2013.06.002

Sahoo S, Zhang S, Shim JJ (2016) Porous ternary high performance supercapacitor electrode based on reduced graphene oxide, NiMn2O4, and polyaniline. Electrochim Acta 216:386–396. https://doi.org/10.1016/j.electacta.2016.09.030

Samodi A, Rashidi A, Marjani K, Ketabi S (2013) Effects of surfactants, solvents and time on the morphology of MgO nanoparticles prepared by the wet chemical method. Mater Lett 109:269–274. https://doi.org/10.1016/j.matlet.2013.07.085

Saranya PE, Selladurai S (2018) Efficient electrochemical performance of ZnMn2O4 nanoparticles with rGO nanosheets for electrodes in supercapacitor applications. J Mater Sci Mater Electron 29:3326–3339. https://doi.org/10.1007/s10854-017-8268-5

Siciliano T, Di Giulio M, Tepore M et al (2009) Ammonia sensitivity of rf sputtered tellurium oxide thin films. Sens Actuators, B Chem 138:550–555. https://doi.org/10.1016/j.snb.2009.02.068

Song XZ, Meng YL, Chen X et al (2018) Hollow NiFe2O4 hexagonal biyramids for high-performance: N-propanol sensing at low temperature. New J Chem 42:14071–14074. https://doi.org/10.1039/c8nj02438c

Sovizi MR (2020) A chemiresistor sensor modified with lanthanum oxide nanoparticles as a highly sensitive and selective sensor for dimethylamine at room temperature. New J Chem 44:4927–4934. https://doi.org/10.1039/c9nj06329c

Su H, Xu Y, Shen S et al (2020) Porous core–shell $CoMn_2O_4$ microspheres as anode of lithium ion battery with excellent performances and their conversion reaction mechanism investigated by XAFS. J Energy Chem 1637:2–9. https://doi.org/10.1016/j.jechem.2018.04.009

Sun L, Jiang L, Hua X et al (2019) Preparation of Au/xCeO2-Al2O3 catalysts with enhanced catalytic properties for the selective acetylene hydrogenation. J Alloys Compd 811:152052. https://doi.org/10.1016/j.jallcom.2019.152052

Type I, Chandra S (2017) Sensing system for salinity testing using laser-induced graphene sensors. Sens Actuators A Phys. https://doi.org/10.1016/j.sna.2017.08.008

Wang L, Wang Y, Tian H et al (2020) Enhanced ammonia detection using wrinkled porous CoFe2O4 double-shelled spheres prepared by a thermally driven contraction process. Sens Actuators, B Chem 314:128085. https://doi.org/10.1016/j.snb.2020.128085

Yu L, Zhong Q, Zhang S et al (2015) A CuO-V2O5/TiO2 catalyst for the selective catalytic reduction of NO with NH3. Combust Sci Technol 187:925–936. https://doi.org/10.1080/00102202.2014.993028

Zhang L, He H (2009) Mechanism of selective catalytic oxidation of ammonia to nitrogen over Ag/Al_2O_3. J Catal 268:18–25. https://doi.org/10.1016/j.jcat.2009.08.011

Zhou J, Ikram M, Rehman AU et al (2018) Highly selective detection of NH_3 and H2S using the pristine CuO and mesoporous In_2O_3@CuO multijunctions nanofibers at room temperature. Sens Actuators, B Chem 255:1819–1830. https://doi.org/10.1016/j.snb.2017.08.200

Zhou T, Cao S, Zhang R et al (2019) Effect of cation substitution on the gas-sensing performances of ternary spinel MCo_2O_4 (M = Mn, Ni, and Zn) Multishelled Hollow Twin spheres. ACS Appl Mater Interfaces 11:28023–28032. https://doi.org/10.1021/acsami.9b07546